Finding Source of Electromagnetic Interference (EMI) to GPS Using a Network Sensors

Shau-Shiun Jan, Per Enge

Department of Aeronautics and Astronautics
Stanford University

ABSTRACT

Any electromagnetic interference (EMI) to GPS must invoke a fast location and removal response, because of the high military and civilian reliance on GPS. In this report, we present an approach, which is based on deploying a network of sensors to estimate the location of EMI source. We believe that this approach provides some unique advantages. First, it includes the possibility of using a terrestrial and/or airborne network for finding interference to airborne receivers. Since a terrestrial network could surround an airport with a continuous interference finding capability, such a network would be much less expensive than monitoring with a continuously airborne fleet of even unmanned air vehicles. It would also provide a quicker response than a strategy based on dispatching aircraft after the onset of interference. Such a terrestrial network need not be expensive since it could be based on an abundance of cheap sensors rather than a few sensors at hardened sites. Second, the combination of different sensors may improve the positioning performance. In particular, our approach is likely to outperform the proposal to estimate interference location by measuring power received by a top-mounted antenna on a banking aircraft.

I. INTRODUCTION

This paper studies the use of a terrestrial and/or airborne sensor network to estimate the location of electromagnetic interference (EMI) sources. Radio systems play an increasing role in our military and civilian infrastructure, and many of these systems are vulnerable to accidental and malevolent EMI attack. Malevolent EMI attack on civil aircraft would not be new, and will probably increase in our society where computer hacking has become a pastime for malcontents. A rapid interference finding capability is needed to protect these systems and mitigate the threat.

This research assumes an EMI attack on GPS aircraft operations. However, our results have broader applicability. GPS is a space-to-earth signal and the received signal power is -160 dBW. This low power level makes GPS highly susceptible to interference. It presently serves around 8 million users in sea, air, terrestrial, and space applications. Many of these applications are safety of life operations. For example, GPS is used to guide ships while approaching harbor and navigating within narrow waterways. GPS also provides guidance in terrestrial emergency applications, such as ambulances and police cars, while they conduct their critical missions. In addition, GPS serves many aviation applications including the most demanding phase of flight – aircraft approach and landing. Most aircraft approach operations allow no more than one missed approach per 100,000 landings. Today, radio frequency interference is the single greatest threat to this continuity of service. The conclusion of the *GPS Risk Assessment Study* by the Applied Physics Laboratory at the Johns Hopkins University: 'the only GPS risks that proved significant are interference and ionosphere propagation effects'.

This work is organized as follows. Section II discusses the prior work in this area. The basics of EMI source position estimation are summarized in Section III. In Section IV, we explain the configurations and assumptions of our work, which uses a network of sensors, and two kinds of sensors are considered. In addition, examples and results are given in Section IV. Section V presents a summary and concluding remarks.

II. PRIOR ART

In this section, we discuss a GPS Interference Source Location and Avoidance Systems which was developed by the U.S. DOT Volpe National Transportation Systems Center [2]. This system is called Aircraft RFI Localization and Avoidance System (ARLAS), and uses a GPS

antenna mounted on the top of an aircraft to detect the location of interference. As shown in Fig. 1, their work for determining the direction of a GPS interference source from an aircraft (ARLAS) exploits the vertical gain pattern of the aircraft's top-mounted GPS antenna. The signal-to-noise ratio (SNR) received at the top-mounted GPS antenna can be calculated by the GPS receiver and the different values of roll, pitch, and heading which are measured by the aircraft gyros. When the aircraft is banked, the antenna illuminates some area on the ground and obscures others. When aircraft flies a tight circle, it can scan the ground and obtain data to estimate the direction to an interference source.

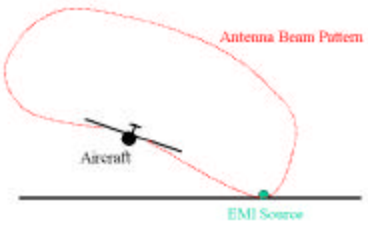

Figure 1. The work of the Volpe National Transportation Systems Center, when the aircraft is banked, the antenna illuminates some area on the ground and obscures others.

The DOT Volpe center flight tested the ARLAS concept in March 1999. This system could not determine the interference's bearing with sufficient reliability to validate the approach. Performance was limited because the ARLAS could not collect sufficient bearing measurements samples simultaneously. Moreover, pilots' dislike the observation maneuvers required for this bearings-only tracking system, because the ARLAS requires multiple turns for normal operation.

Based on the results of the DOT Volpe center flight test, we propose the use of sensor networks to estimate the location of electromagnetic interference (EMI) sources. The network of distributed sensors has several advantages. First, we can place the sensors to give good performance for any interferers near the airport. Secondly, an optimal observer maneuver is not required because the requisite geometric diversity of measurements can be achieved by proper location of the network of distributed sensors. In this research, we prefer a terrestrial network, but the analysis is also applicable to airborne sensors which could be used to augment the ground network.

III. BASICS OF POSITION ESTIMATION

The concept of locating a stationary EMI source from passive measurements can be found in a wide variety of radar and sonar publications [1, 2, 3, 4]. The location of an EMI source can be estimated either by a network of distributed sensors or by a single sensor. There are at least two methods to estimate the emitter location. The conventional method is based on different bearing measurements at different points along the sensor trajectory. The other method is to measure the Doppler shift of the EMI source frequency caused by the relative motion between the sensor and the EMI source.

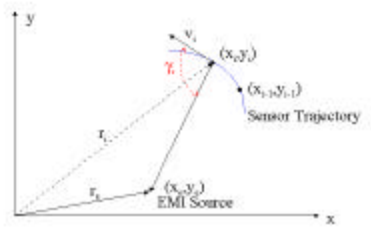

Figure 2. An example two-dimensional geometry of the sensor and the EMI source

As shown in Fig. 2, (x_e, y_e) is the unknown two-dimensional position of the stationary EMI source, (x_i, y_i) is the known sensor position at the i^{th} epoch. The velocity of sensor is $v_i = (\dot{x}_i, \dot{y}_i)$, and g_i is the noise free bearing measurement to the EMI source relative to the velocity vector of the sensor. We assume that f_i is the Doppler shifted but noise free signal frequency at the i^{th} measurement point along the sensor trajectory, c is the speed of light, and f_0 is the transmitted signal frequency. The relations between these parameters are

$$g_i = \cos^{-1}\left[\frac{v_i \cdot (r_e - r_i)}{|v_i| \cdot |r_e - r_i|}\right] = \cos^{-1}\left[\frac{\dot{x}_i \cdot (x_e - x_i) + \dot{y}_i \cdot (y_e - y_i)}{\sqrt{\dot{x}_i^2 + \dot{y}_i^2} \cdot \sqrt{(x_e - x_i)^2 + (y_e - y_i)^2}}\right] \quad (1)$$

and

$$f_i = f_0 + \frac{f_0}{c}\cdot\frac{v_i\cdot(r_e - r_i)}{|r_e - r_i|} = f_0 + \frac{f_0}{c}\cdot\frac{\dot{x}_i\cdot(x_e - x_i) + \dot{y}_i\,(y_e - y_i)}{\sqrt{(x_e - x_i)^2 + (y_e - y_i)^2}} \quad (2)$$

With additive noise, either observation equation can be written as

$$j^m = j(a) + n \quad (3)$$

where, j^m is the measured bearing or frequency,

$j(a)$ is the true (noise free) bearing or frequency,

$a_B = \begin{bmatrix} x_e \\ y_e \end{bmatrix}$ for bearing measurements,

$a_F = \begin{bmatrix} f_0 \\ x_e \\ y_e \end{bmatrix}$ for frequency measurements,

n are measurement errors.

If the EMI transmitted frequency is unknown, we will need to estimate f_0 as well. This is why a_F includes f_0. The measurement noise n is assumed to be zero mean ($E[n_B] = E[n_F] = 0$) with a normal probability distribution, and the measurements are independent of each other. Therefore, the variances are independent of the measurement points, that is, the covariance matrices for this two dimensional example are

$$N_B = E[(n_B - E[n_B])(n_B - E[n_B])^T]$$
$$\because E[n_B] = 0, (N_B)_{ij} = 0, (N_B)_{ii} = s_B^2$$
$$\Rightarrow N_B = E[(n_B)(n_B)^T] = \begin{bmatrix} s_B^2 & 0 \\ 0 & s_B^2 \end{bmatrix}$$
$$N_F = E[(n_F - E[n_F])(n_F - E[n_F])^T]$$
$$\because E[n_F] = 0, (N_F)_{ij} = 0, (N_F)_{ii} = s_F^2$$
$$\Rightarrow N_F = E[(n_F)(n_F)^T] = \begin{bmatrix} s_F^2 & 0 \\ 0 & s_F^2 \end{bmatrix}$$

where, the subscript B is for bearing measurements, and the subscript F is for frequency measurements. We assume that the measurement noise follows a Gaussian distribution. As a result, we can write the conditional probability distribution of the measurements as follows

$$p\langle j^m | a\rangle = \frac{1}{(2p)^{M/2}\sqrt{\det N}}\exp\left(-\frac{1}{2}\sum_{i=1}^{M}\frac{(j_i^m - j_i(a))^2}{N_{ii}}\right) \quad (4)$$

The Cramer-Rao inequality provides a lower bound on the estimation accuracy. We define the estimation error as

$$\hat{\Delta a} = \hat{a}(j^m) - a \quad (5)$$

where, $\hat{\Delta a}$ is estimation error,

$\hat{a}(j^m)$ is the unbiased estimate of a.

The covariance matrix of the estimation error, C, is bounded by the inverse of the Fisher information matrix, J. Specifically, $C \geq J^{-1}$, where

$$J_{kl} = -E\left[\frac{\partial^2 \ln p\langle j^m | a\rangle}{\partial a_k \partial a_l}\right]$$

The covariance matrix can be represented geometrically in the space as an ellipse that bounds the estimation errors. That is,

$$\hat{\Delta a}^T C^{-1} \hat{\Delta a} = k \quad (6)$$

where, k is a constant which determines the size of the ellipse.

From $C \geq J^{-1}$, we can rewrite (6) as

$$\hat{\Delta a}^T J \hat{\Delta a} = k \quad (7.1)$$

$$\hat{\Delta a}^T J \hat{\Delta a} = \sum_{i=1}^{n} l_i x_i^2 = k \quad (7.2)$$

where, l_i are the eigenvalues of J,

x_i are the corresponding eigenvectors.

The size and orientation of the error ellipse can be described in terms of the eigenvalues (l_i) and the eigenvectors (x_i) of the Fisher Information matrix. If l_i is zero, then the length of the semiaxes of the ellipse is infinite, that means, it is an unobserved state. If l_i is not zero, then the length of the semiaxes of the ellipse is $\sqrt{k/l_i}$.

To derive the elements of the Fisher Information matrix, we take the logarithm and differentiate

$$J_{kl} = -E\left[\frac{\partial^2 \ln p\left\langle j^{\,m} \middle| a\right\rangle}{\partial a_k \partial a_l}\right] = \sum_{i=1}^{M} \frac{1}{N_{ii}} \cdot \frac{\partial j_i}{\partial a_k} \cdot \frac{\partial j_i}{\partial a_l} \quad (8)$$

or rewrite it in matrix form

$$J = \sum_{i=1}^{M} \frac{1}{N_{ii}} \nabla_a j_i \left(\nabla_a j_i\right)^T \quad (9)$$

where, ∇_a is the gradient with respect to a.

$\nabla_{a_B} = \left(\frac{\partial}{\partial x_e}, \frac{\partial}{\partial y_e}\right)^T$ for bearing measurements.

$\nabla_{a_F} = \left(\frac{\partial}{\partial f_0}, \frac{\partial}{\partial x_e}, \frac{\partial}{\partial y_e}\right)^T$ for frequency measurements.

For bearing measurements, we find

$$\nabla_{a_B} g_i = \left(\frac{\partial g_i}{\partial x_e}, \frac{\partial g_i}{\partial y_e}\right)^T = \frac{1}{\left|r_e - r_i\right|^2} \cdot \begin{pmatrix} y_i - y_e \\ x_e - x_i \end{pmatrix} \quad (10)$$

For frequency measurements, we find

$$\nabla_{a_F} f_i = \left(\frac{\partial f_i}{\partial f_0}, \frac{\partial f_i}{\partial x_e}, \frac{\partial f_i}{\partial y_e}\right)^T = \begin{pmatrix} 1 + \frac{1}{c \cdot \left|r_e - r_i\right|} \cdot \left(\dot{x}_i \cdot \left(x_e - x_i\right) + \dot{y}_i \cdot \left(y_e - y_i\right)\right) \\ \frac{c}{f_0} \cdot \frac{y_e - y_i}{\left|r_e - r_i\right|^3} \cdot \left(\dot{x}_i \cdot \left(y_e - y_i\right) + \dot{y}_i \cdot \left(x_e - x_i\right)\right) \\ \frac{c}{f_0} \cdot \frac{x_e - x_i}{\left|r_e - r_i\right|^3} \cdot \left(\dot{y}_i \cdot \left(x_e - x_i\right) + \dot{x}_i \cdot \left(y_e - y_i\right)\right) \end{pmatrix} \quad (11)$$

We give two examples to illustrate the single measurement case. Fig. 3 shows the initial sensor position and the EMI source position.

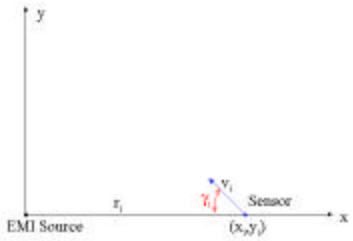

Figure 3. An example two-dimensional geometry of the sensor and the EMI source

A. Single Bearing Measurement Example

From equation (9), we can drive the Fisher Information matrix as

$$J = \frac{1}{s_B^2} \cdot \nabla_{a_B} g \left(\nabla_{a_B} g\right)^T \quad (12)$$

From Fig. 3, we can compute (10) to get

$$\nabla_{a_B} g = \frac{1}{r} \begin{pmatrix} 0 \\ -1 \end{pmatrix} \quad (13)$$

Substituting (12) into (13), we get

$$J = \frac{1}{s_B^2 r^2} \cdot \begin{pmatrix} 0 & 0 \\ 0 & 1 \end{pmatrix} \quad (14)$$

The eigenvalues and the corresponding eigenvectors of J are

$$\begin{aligned} l_1 &= 0 \\ l_2 &= \frac{1}{s_B^2 r^2} \\ x_1 &= \begin{pmatrix} 1 \\ 0 \end{pmatrix} \\ x_2 &= \begin{pmatrix} 0 \\ 1 \end{pmatrix} \end{aligned} \quad (15)$$

Then we calculate the length of the semiaxes

$$\begin{aligned} d_1 &= \infty \\ d_2 &= \sqrt{\frac{k}{l_2}} \end{aligned} \quad (16)$$

The result of this example is shown in Fig. 4, and it is a strip in the line of sight direction with $2d_2$ width. The multiple measurements case can be interpreted as the result of the intersection of several such individual strips.

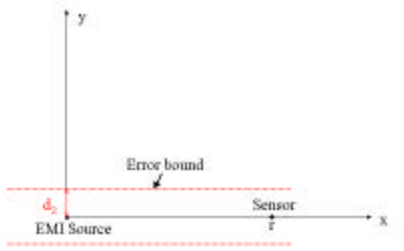

Figure 4. The result of the single bearing measurement example

B. Single Frequency Measurement Example

If the sensor in Fig. 2 uses frequency measurements instead of bearing measurements, then we derive the Fisher Information matrix from equation (9) as follows

$$J = \frac{1}{s_F^2} \cdot \nabla_{a_F} f (\nabla_{a_F} f)^T \tag{17}$$

Based on Fig. 2, we can calculate (10) and get

$$\nabla_{a_F} f = \begin{bmatrix} 1+\frac{1}{c\cdot|r_e - r_i|^3}\cdot(\dot{x}_i\cdot(x_e - x_i)+\dot{y}_i\cdot(y_e - y_i)) \\ \frac{c}{f_0}\cdot\frac{y_e - y_i}{|r_e - r_i|^3}\cdot(\dot{x}_i\cdot(y_e - y_i)+\dot{y}_i\cdot(x_e - x_i)) \\ \frac{c}{f_0}\cdot\frac{x_e - x_i}{|r_e - r_i|^3}\cdot(\dot{y}_i\cdot(x_e - x_i)+\dot{x}_i\cdot(y_e - y_i)) \end{bmatrix} \tag{18}$$

$$= \begin{bmatrix} 1+\frac{1}{cr}\cdot((-v_i\cos g_i)\cdot(-r)) \\ 0 \\ \frac{f_0}{c}\cdot\frac{-r}{r^3}\cdot((v_i\sin g_i)\cdot(-r)) \end{bmatrix} = \begin{bmatrix} 1+\frac{1}{c}\cdot(v_i\cos g_i) \\ 0 \\ \frac{f_0}{cr}\cdot(v_i\sin g_i) \end{bmatrix}$$

Then substitute (17) into (18), we get the Fisher Information matrix

$$J = \frac{f_0^2}{s_F^2}\cdot P \tag{19}$$

where,

$$P = \begin{bmatrix} u^2 & 0 & uw \\ 0 & 0 & 0 \\ uw & 0 & w^2 \end{bmatrix}$$

$$u = \frac{1}{f_0}\cdot\left(1+\frac{v_i}{c}\cdot\cos g_i\right)$$

$$w = \frac{v_i}{cr}\cdot\sin g_i$$

The eigenvalues and the corresponding eigenvectors of J are

$$\begin{aligned} &l_1 = u_2 + w_2,\ l_2 = l_3 = 0 \\ &x_1 = \frac{1}{\sqrt{u^2+w^2}}\cdot\begin{bmatrix} u \\ 0 \\ w \end{bmatrix} \\ &x_2 = \begin{bmatrix} 0 \\ 1 \\ 0 \end{bmatrix} \\ &x_3 = \frac{1}{\sqrt{u^2+w^2}}\cdot\begin{bmatrix} -w \\ 0 \\ u \end{bmatrix} \end{aligned} \tag{20}$$

Then we compute the length of the semiaxes

$$\begin{aligned} &d_1 = \frac{s_F\cdot\sqrt{k}}{f_0\cdot\sqrt{u^2+w^2}} \\ &d_2 = \infty \\ &d_3 = \infty \\ &\cos q = x_1\cdot e_y = \frac{w}{\sqrt{u^2+w^2}} \\ &q = \cos^{-1}\left(\frac{w}{\sqrt{u^2+w^2}}\right) \end{aligned} \tag{21}$$

The result is shown in Fig. 5. It is a disk in the position and frequency space, and we plot the projection on the $\hat{f} - y$ plane. The angle q between the eigenvector x_1 and the line of sight can be computed from equation (21).

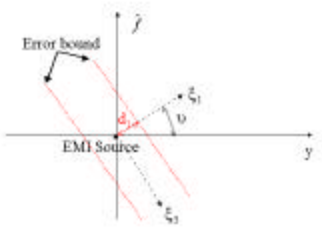

Figure 5. The result of the single frequency measurement example

The results of the previous two examples, can be used to predict positioning accuracy for a system that uses multiple sensors or one moving sensor, as shown in Fig. 6.The smaller area of

intersection of the strips gives the better bearing tracking performance. Fig. 7 shows that the optimal observer maneuver is required for the better tracking performance.

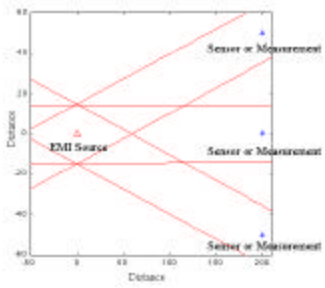

Figure 6. The sufficient measurements are required to locate the EMI source

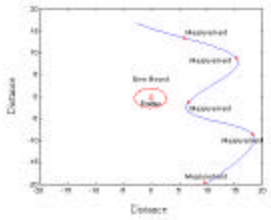

Figure 7. The optimal observer maneuver is required for the better tracking performance

IV. NETWORK OF SENSORS

In this section, we characterize the performance of a network of distributed sensors with respect to the following parameters: number of sensors, distance between sensors and interference source, separation of the sensors, and geometry of the sensors. An example network of sensors is shown in Fig. 8.

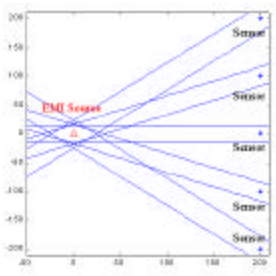

Figure 8. An example of network of sensors

A. Multiplicity of Sensors and Sensor Span

The first example investigates the relation between bearing tracking performance and the number of sensors. We consider two networks, one with three sensors, and the other with seven sensors. The separations of the sensors are same in both systems, and the seven sensors system spans triple the distance. These networks are shown in Fig. 9. The bearing tracking performance (accuracy) of the network system with seven sensors is better than that of the network system with three sensors because the span of the network system with seven sensors is triple that of the network system with three sensors. Consequently, the network system with seven sensors is better than that of the network system with three sensors.

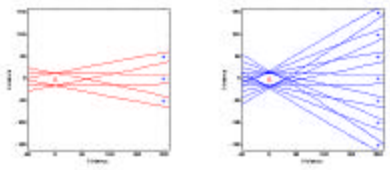

Figure 9. The comparison in the different numbers of sensors, the bearing tracking performance of the network system with seven sensors (on the right) is better than that of the network system with three sensors (on the left).

B. Distance from Sensors to EMI Source

The second example investigates how the distances between the EMI source and the sensors can affect the bearing tracking performance. We have two systems, and both systems are five sensors networks. The distance from the EMI source to the first network of sensors is $1/4$ of the distance from the same EMI source to the second network of sensors. Again, the separations of the sensors are equal. The bearing tracking performance of the nearby network system is better than the performance of the distant network system. The larger geometry diversity of the nearby network gives the better bearing tracking performance. The result is shown in Fig. 10.

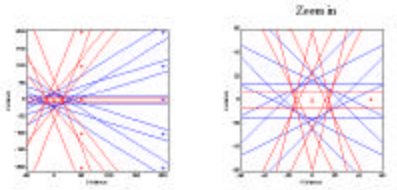

Figure 10. The comparison in the different distances from EMI source to the sensors, the system, which is near the EMI source, gives the better bearing tracking performance because of the larger geometry diversity.

C. Sensor Separation

The third example tests the separations of the sensors. The results are shown in Fig. 11. As expected the network with the larger span gives the better bearing tracking performance. This is also the reason why the conventional bearing-only tracking systems require maneuvers. They need to get bearing measurements over a long span of distance. In our approach, we only need to make sure that the separations of sensors are large enough to fulfill certain performance requirements. This is an advantage of our approach because no optimal maneuver is needed.

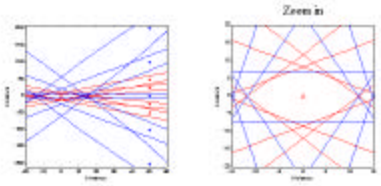

Figure 11. The comparison in the different separations of the sensors, the larger geometry diversity of the network of sensors gives the better bearing tracking performance.

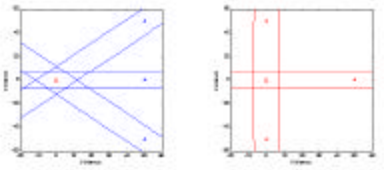

Figure 12. The comparison in the different geometries of the sensors, the smaller area of the intersection of the ellipses gives the better bearing tracking performance.

D. Sensor Failure

The fourth example illustrates how the geometry of the distributed sensors can improve the bearing tracking performance, and the design of networks that are robust to sensor failures. As shown in Fig. 12, the left-hand network of sensors is distributed in a straight line, and the right-hand network of sensors is distributed in a triangular shape. The right-hand network system has greater geometric diversity than the left-hand network system. Therefore, the right-hand network of sensors gives the better bearing tracking performance. The result of this example suggested that we might be able to maintain the bearing tracking performance when some of the sensors were failed by moving existing sensors to form the better geometry. For instance, we can remove one sensor on the top of EMI source from the right-hand network system in Fig. 12, and we get the same bearing tracking performance as before. That is, when one of the sensors in the left-hand network has failed, we can move the two existing sensors to be in the geometry of the right-hand network system to maintain bearing tracking performance. Actually, this performance is better than the original system, as shown in Fig. 13. As shown, the network is robust to sensor failures.

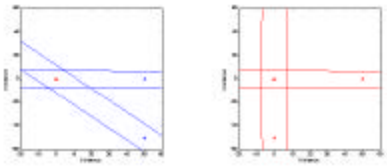

Figure 13. An example of the network system in the presence of sensor failures, we can maintain the bearing tracking performance when some of the sensors were failed by moving existing sensors to form the better geometry.

V. CONCLUDING COMPARISON

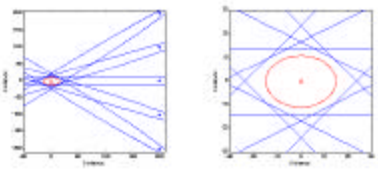

Figure 14. Comparison example between the prior art and our approach

As shown in Fig. 14, the red error ellipse is the result of the five sequential bearing measurements by using single sensor, and the blue strips are the results of the five individual bearing measurement from five different sensors. The area of the intersection of the blue strips is almost same as that of the red error ellipse. However, It is very difficult to achieve this bearing tracking performance (the red error ellipse) by using a single sensor, because EMI source may turn off before maneuver is completed.

Our approach to locate the EMI source by using a network of sensors has two major advantages: (1) No sensor motion is needed, and EMI source location is estimated instantaneously. We can simply change the separations of the sensors or the geometry of the sensors to fulfill the bearing tracking performance requirements, (2) It is robust to sensor failures. That is, even when some of the sensors are failed, we can maintain the bearing tracking performance by moving existing sensors to form better sensors' geometry.

ACKNOWLEDGMENT

The authors would like to thank the Charles Stark Draper Laboratory for sponsoring this research.

REFERANCES

1. A. Brown, D. Reynolds, and D. Robert, "Jammer and Interference Location System-Design and Initial test Results", *Proceedings of The ION 55th Annual Meeting*, June 1999.

2. B. M. Winer, P. Manning, E. M. Geyer, J. Ruggiero, and P. McCarty, "GPS Interference Source Location and Avoidance Systems", *Proceedings of The ION 53rd Annual Meeting*, June 1997.

3. J. E. Wohlfiel, B. Tanju, "Location of GPS Interference", *Proceedings of The ION GPS '99*, September 1999.

4. K. Becker, "An Efficient Method of Passive Emitter Location", *IEEE Transactions on Aerospace and Electronic Systems*, Vol. 28, NO. 4, October 1992.

5. K. Gromov, D. Akos, S.Pullen, P. Enge, B. Parkinson, and B. Pervan, "Interference Direction Finding for Aviation Applications of GPS", *Proceedings of The ION GPS '99*, September 1999.

6. S.-S. Jan, and P. Enge, "Using GPS to Synthesize A Large Antenna Aperture when the Elements are Mobile", *Proceedings of The ION NTM 2000*, January 2000.

7. T. M. Corrigan, J. F. Hartranft, L. J. Levy, K. E. Parker, J. E. Pritchett, A. J. Pue, S. Pullen, and T. Thompson, *GPS Risk Assessment Study Final Report*, the Johns Hopkins University, January 1999.

BIOGRAPHY

Shau-Shiun Jan is a Ph.D. candidate in the Department of Aeronautics and Astronautics at Stanford University. He received his M.S. degree in Aeronautics and Astronautics from Stanford University in 1998.

Per Enge is a professor in the Department of Aeronautics and Astronautics at Stanford University. He received his M.S. and Ph.D. from University of Illinois at Champaign Urbana. He is Principle Investigator for the LAAS and WAAS laboratories at Stanford.